International Forum on Aeroelasticity and Structural Dynamics
IFASD 2024
17−21 June 2024, The Hague, The Netherlands

EVALUATION OF AEROELASTIC MODELS FOR GUST RESPONSE PREDICTION IN VERY FLEXIBLE WINGS

Divya Sanghi[1], **Cristina Riso**[2], **Carlos E. S. Cesnik**[1]

[1]University of Michigan
Ann Arbor, MI, 48109
dsanghi@umich.edu, cesnik@umich.edu

[2]Georgia Institute of Technology
Atlanta, GA, 30332
criso@gatech.edu

Keywords: Aeroelastic prediction; gust response; very flexible wing; large deflections.

Abstract: This paper compares aeroelastic models for gust response prediction in very flexible wings. The investigations focus on the Pazy wing benchmark developed at Delft University of Technology for gust response experiments in low-speed flow. The comparisons consider two geometrically nonlinear aeroelastic models of the wing, which comprise an equivalent beam representation of the structure coupled with unsteady potential flow aerodynamics based on either strip theory with wingtip corrections or the vortex-lattice method. The study examines wing responses to 1-cosine vertical gust inputs for various maximum gust velocities, flow speeds, and root angles of attack, exciting a wide range of deflections. The aeroelastic models based on corrected strip theory and the unsteady vortex-lattice method predict maximum wing tip vertical displacements that differ by less than 3%. The models also agree on the characteristic frequency and phase during the free decay after the gust. However, the model based on strip theory predicts a faster free decay due to higher aerodynamic damping, consistent with findings from previous flutter investigations focused on the Technion Pazy wing. These results provide new insights into the impact of model complexity on aeroelastic prediction accuracy for very flexible wings, expanding the scope of previous studies to encompass gust responses.

1 INTRODUCTION

In the aerospace industry, there is a trend towards novel aircraft configurations characterized by lighter-weight, more slender, and higher-aspect-ratio wings [1, 2]. This trend stems from the pressing demand for aircraft that can support the continued growth of the aviation system while reducing its environmental impacts [3]. Lightweight, slender, high-aspect-ratio wings enhance aircraft energy efficiency thanks to their lower induced drag and empty weight, contributing to making aggressive sustainable aviation goals achievable [2]. However, these wings experience large aeroelastic deflections under normal operating loads due to the increased flexibility of lightweight structures and high-aspect-ratio geometries. As a result, these very flexible wings require a shift in current aircraft industrial design practices, which rely on models and analysis methods that do not capture wing aeroelastic behaviors in the presence of large deflections [4]. To design future aircraft with lighter-weight, more slender, and higher-aspect-ratio wings, it is necessary to establish trusted geometrically nonlinear approaches that can accurately capture these behaviors at a tractable computational burden.

Geometrically nonlinear effects associated with large aeroelastic deflections manifest in three main ways [5]. Firstly, in the presence of large deflections, wings exhibit so-called shortening effects under the effect of applied loads. These effects are associated with non-negligible displacement components in other directions than the primary direction along which the structure is loaded (e.g., transverse direction for wings), causing structural points to move along curved paths during deformation instead of the straight paths expected under linear assumptions. This situation requires evaluating aerodynamic loads in the deformed shape and accounting for their follower nature, in contrast with the linear approach of evaluating them on the undeformed shape and neglecting any changes in their orientation. Secondly, large deflections make the wing's *modal* scenario (natural frequencies and mode shapes) change with the deformed shape. As a result, the modal scenario of the wing becomes a function of the operating condition. Lastly, the combination of these effects makes the *stability* scenario also vary with the deformed shape, which is again a function of the operating condition.

In 2019, the Third Aeroelastic Prediction Workshop (AePW3) Large Deflection Working Group (LDWG) was established to address the aeroelastic modeling and analysis challenges associated with very flexible wings. The LDWG sought to evaluate aeroelastic modeling and analysis capabilities currently available for these wings and fundamentally understand their advantages and limitations. The activities focused on the Pazy wing [6], an aeroelastic benchmark wing case for geometrically nonlinear aeroelastic experiments involving large deflections in low-speed flow. The unique feature that sets the Pazy wing apart from other previous aeroelastic experimental models (e.g., Ref. [7]) is its ability to sustain structural and aerodynamic loads that induce tip vertical displacements up to 50% of the semispan. This feature has enabled static and flutter tests at unprecedented deflections [6, 8], providing the community with deeper insights into aeroelastic physics in these conditions as well as a comprehensive public experimental database for model validation. The simplicity of the Pazy wing configuration and availability of large-deflection validation data has facilitated extensive experimental-numerical correlations focused on the ability of various geometrically nonlinear aeroelastic models to predict modal scenarios, static responses, and flutter boundaries of very flexible wings at low speeds [5].

Among the key conclusions from LDWG comparisons, low-order geometrically exact beam models with equivalent inertia and stiffness properties derived by a built-up finite element model (FEM) were found to predict wing deflections with the same accuracy as the parent higher-order model while only requiring a small fraction of the degrees of freedom (DOFs) [5]. These low-order models were also found to be more numerically robust and converge in cases where a built-up FEM would struggle or fail. When geometrically exact beam models are coupled to aerodynamic models based on unsteady potential flow strip theory, the resulting low-order aeroelastic models accurately predict wing static aeroelastic responses up to extreme deflections compared with higher-order models based on more sophisticated aerodynamic theories, as long as wingtip effects are captured [9]. Different approaches are possible for this, from analytical tip loss factors [9] to spanwise varying aerodynamic coefficient distributions [10]. However, aeroelastic solutions based on corrected strip theory yield larger flutter prediction errors, especially for flutter points that shift significantly for small aerodynamic damping changes (such as the ones associated with hump modes) [9]. Interestingly, flutter points at lower wing deflections are less accurately captured by strip-theory-type aerodynamics, with increased sensitivity to the approach used to account for wingtip effects [9, 10]; flutter points at larger wing deflections are predicted more accurately, suggesting a stronger role of structural geometrical nonlinearities (due to changes in the modal scenario) over three-dimensional unsteady aerodynamics [10].

The above findings raise the question of how geometrically nonlinear aeroelastic models based on aerodynamic models of different complexity capture other metrics for very flexible wings. One such metric is the dynamic response to gust loads, which are typical load cases considered for aircraft aeroelastic qualification. To the authors' knowledge, only limited studies have investigated gust responses of very flexible wings, none of which has focused on understanding the impact of model complexity on aeroelastic prediction accuracy. For instance, del Carre et al. [11] compared two low-order flight dynamics-nonlinear aeroelastic frameworks for lateral gust responses of a very flexible aircraft in free flight, observing close agreement. However, the compared frameworks involved similar modeling approaches, a geometrically exact beam theory for the structure, and the unsteady vortex-lattice method (UVLM) for aerodynamics. More recently, Ribeiro et al. [12] correlated gust response simulations for a variant of the Pazy wing developed at Delft University of Technology (TU Delft) with experimental data [13]. The model used to conduct the simulations consisted of a geometrically exact beam theory coupled with a free-wake panel method. The study found that amplitude and phase errors in predicting wing tip vertical displacements due to a sinusoidal gust originated from the wing induction at the experimental measurement location, with improved correlations when accounting for this effect in simulations. However, the study did not compare gust response results with alternative numerical solutions. Riso and Cesnik [9, 10] investigated the impact of aeroelastic model complexity on prediction accuracy for very flexible wings, but only considered modal, static, and flutter metrics.

This paper investigates the gust responses of a very flexible wing using aeroelastic models of different levels of complexity. The paper focuses on evaluating the impact of different unsteady potential flow aerodynamic theories on the resulting gust response predictions. The investigations focus on the TU Delft Pazy wing, with the ultimate goal of comparing simulation results from the numerical models presented here with experimental data (in future research). The models leverage the University of Michigan's Nonlinear Aeroelastic Simulation Toolbox (UM/NAST) [14], a multidisciplinary framework for modeling, analyzing, and simulating very flexible wings and aircraft. The study compares two models, which are developed, verified, and validated following a previously established workflow [9, 10]. These models share a common equivalent beam representation of the parent built-up FEM of the TU Delft Pazy wing based on the geometrically exact strain-based formulation of Su and Cesnik [15]. This geometrically exact beam model is coupled with an unsteady potential flow aerodynamic model based on either strip theory with wingtip corrections (resulting in a low-oder aeroelastic model) or the UVLM (resulting in a medium-order aeroelastic model). The two models are compared for wing responses to 1-cosine vertical gust inputs considering various gust velocity magnitudes and operating conditions, which are selected to excite a wide range of static, dynamic, and total deflections. The resulting findings contribute to a growing understanding of the impact of model complexity on aeroelastic prediction accuracy for very flexible wings, expanding the scope of previous studies to include gust responses.

The remainder of this paper is organized as follows: Sec. 2 briefly describes UM/NAST, focusing on the aspects that are necessary to understand the results; Sec. 3 describes the TU Delft Pazy wing experimental benchmark case and the numerical models used in this work; Sec. 4 discusses the model verification and gust response results; and the final section draws concluding remarks.

2 COMPUTATIONAL FRAMEWORK

This study leverages UM/NAST [14], a multidisciplinary framework for modeling, analyzing, and simulating very flexible wings and aircraft by capturing coupling effects among structural dynamics, rigid-body dynamics, and steady or unsteady aerodynamics. The main capabilities of the framework are recalled below and further detailed in Refs. [14, 15].

UM/NAST models each structural component (e.g., wing) as a non-isotropic beam member that undergoes arbitrary deflections relative to a body-fixed frame. Elastic deflections are modeled using the geometrically exact, strain-based beam formulation of Su and Cesnik [15], which assumes four strain DOFs per beam element: axial extension, twist, and out-of-plane and in-plane bending curvatures. Shear effects are condensed via energy minimization [16], leading to a 4×4 cross-sectional constitutive law between the axial, torsion, and bending strain measures and the cross-sectional stress resultants (axial force, twisting moment, and bending moments, respectively). Once the model strain vector is known, the deformed shape is recovered by marching the kinematic relations in space [14, 15].

The UM/NAST strain-based formulation can be coupled with various steady or unsteady aerodynamic models available either as built-in options in UM/NAST or as external solvers that can be interfaced with the framework. These models include unsteady potential flow strip theory with various wingtip corrections and the UVLM, which are used in this work. The aeroelastic equations can be further coupled with rigid-body dynamics equations for analyzing and simulating complete aircraft in free flight. However, the rigid-body equations are not used in this work, which focuses on an isolated wing.

This study leverages the UM/NAST modal, static, and dynamic solvers. The first two solvers are used to verify the UM/NAST wing model following the process used in Ref. [9]. The verification also considers results from relevant Nastran solution sequences [17–19]. The UM/NAST dynamic solver is then used to compare gust responses predicted by different aeroelastic models.

3 WING BENCHMARK CASE

3.1 Experimental Model

This work focuses on the TU Delft Pazy wing [13], a variant of the Pazy wing benchmark case [6] originally designed at the Technion for aeroelastic experiments at large deflections in low-speed flow. Both wings have span $\ell = 0.55$ m, chord $c = 0.1$ m, and a uniform NACA0018 airfoil section with no sweep or twist. The wing structure features a plate-like aluminum spar, a 3D-printed nylon frame, an Oralight skin, and a 0.3-m rod to induce flutter and alter the wing dynamics by attaching non-structural weights. TU Delft Pazy wing only differs from the Technion wing in the reduced spar thickness, which allows the wing to achieve similar aeroelastic deflections at lower wind-tunnel flow speeds [13]. The experimental model is detailed in Ref. [13].

While Ref. [13] presented experimental data for the TU Delft Pazy wing gust responses due to a sinusoidal vertical gust, this work does not conduct experimental-numerical correlations. Instead, the work focuses on evaluating different aeroelastic models of the wing for a simpler 1-cosine gust profile as a step toward comparing simulation results with the experimental data in Ref. [13] for a sinusoidal gust profile in future research.

Table 1: Built-up FEM versions and natural frequencies.

	Flexible rod			Rigid rod	
	Original [13]	Updated		Updated	
Mode	Freq. (Hz)	Freq. (Hz)	Δ_{12} (%)	Freq. (Hz)	Δ_{23} (%)
Out-of-plane bending (OOP1)	3.30	3.43	3.91	3.43	0.00
Out-of-plane bending (OOP2)	21.90	22.79	4.04	22.81	0.10
Torsion (T1)	28.10	30.73	9.35	31.29	1.82
Out-of-plane bending (OOP3)	63.10	65.44	3.71	65.85	0.62
In-plane bending (IP1)	n.a.	106.03	n.a.	106.29	0.24
Torsion (T2)	105.90	110.37	4.42	118.29	7.17

3.2 Numerical Model

The UM/NAST low-order model of the TU Delft Pazy wing is developed following the steps in Ref. [9], which were established to model the original Technion wing in the framework. This section summarizes these steps and refers the reader to the previous publication for details.

The first modeling step involves creating the beam structural model of the wing starting from the built-up FEM provided by TU Delft [13], which was updated with ground vibration test (GVT) data. While model updating with GVT data was conducted at TU Delft before this work, they are discussed here to avoid confusion among different existing variants of the built-up FEM and their natural frequencies.

The initial built-up FEM of the TU Delft Pazy wing was derived from the built-up FEM of the original Technion wing by adjusting the spar properties to account for the lower thickness of this variant of the configuration [13]. The first few natural frequencies of this built-up FEM are reported in Table 1 of Ref. [13] along with their comparison with the GVT natural frequencies of the experimental model. The built-up FEM used as the starting point for this work is a more recent version also developed at TU Delft. Different from the first version, this model has no skin and a readjusted spar thickness to best match the GVT natural frequencies after removing the skin elements. The motivation for removing the skin elements was partly to circumvent property uncertainties when modeling the skin using shells and partly to enable using the built-up FEM in nonlinear finite element analyses, where shell elements were found to pose numerical convergence issues [9]. This second built-up FEM version provided by TU Delft was further modified in this work by making the tip rod rigid to ease the process of obtaining equivalent beam properties for UM/NAST. For completeness, Table 1 reports the first six natural frequencies of the three built-up FEM versions in their undeformed shape obtained using the Nastran linear modal analysis solver SOL 103 [17]. The quantity Δ_{12} is the variation in the natural frequencies of the second built-up FEM provided by TU Delft compared with the first one reported in Ref. [13], while the quantity Δ_{23} is the additional variation in the natural frequencies of the second built-up FEM version when making the tip rod rigid in this work. The second built-up FEM has 4% higher OOP and T2 frequencies and a 9% higher T1 frequency compared with the version of Ref. [13]. The IP1 frequency variation is not quantified because its value for the initial built-up FEM was not reported [13]. Making the tip rod rigid does not significantly impact the bending natural frequencies, which increase by less than 1%. However, it increases the T1 and T2 frequencies by 2% and 7%, respectively.

The remainder of this paper considers the built-up FEM of the TU Delft Pazy wing with the rigid tip rod (namely, with the modal characteristics in the last two columns of Table 1). This built-up FEM is used to derive an equivalent beam structural model for UM/NAST using the University of Michigan's Enhanced FEM2Stick (UM/EF2S) framework [20]. Following Ref. [9], the beam reference axis is set at 44% chord in the airfoil symmetry plane and is discretized using 15 strain-based beam elements corresponding to 60 strain DOFs, for a structural model order reduction factor of 315 compared with the built-up FEM. The equivalent beam inertia properties consist of rigid-body elements at the ends of each beam element. Each rigid-body element is defined by a mass, offset from its corresponding node on the beam reference axis, and inertia tensor about the local center of mass. UM/EF2S obtains these quantities based on the built-up FEM mass matrix using a numerically exact process. As a result, any inaccuracies in the equivalent beam structural model are solely due to the numerical discretization and the approximations associated with obtaining the stiffness properties. These properties consist of the cross-sectional stiffness matrix elements of the strain-based formulation of Ref. [15], giving the axial, torsional, out-of-plane bending, and in-plane bending stiffness constants along with the corresponding off-diagonal coupling terms. UM/EF2S obtains the elemental stiffness matrices based on six linearly independent static solutions of the built-up FEM for small deflections about a reference shape, typically the undeformed shape. The equivalent beam inertia and stiffness properties of the TU Delft Pazy wing used in this work are publicly available for download from the authors' GitHub repository[1]. This repository also contains the equivalent beam properties for the Technion wing and the results from studies on the same.

The second and last modeling step involves coupling the structural model with an aerodynamic model. This work considers two options, a built-in low-order model in UM/NAST and an external medium-order model. The low-order model is based on the potential flow thin airfoil theory of Peters et al. [21] and consists of 15 spanwise strips, each associated with a beam element. This model does not add any DOFs in static aeroelastic calculations. However, it adds 90 aerodynamic DOFs in dynamic calculations due to the presence of six inflow states per strip and corresponding evolution equations to capture unsteady wake effects. The model does not require any coupling scheme because it provides aerodynamic loads at the beam element nodes. The formulation accounts for wingtip effects following the approach of Ref. [10], which is based on spanwise-variable aerodynamic coefficient derivatives based on a rigid panel-method analysis of the undeformed Technion Pazy wing at root angle of attack α_r = 1 deg. These aerodynamic coefficient derivatives are given in Ref. [10] and also hold for the TU Delft Pazy wing as the two wings share the same aerodynamic shape. The medium-order model is based on the (U)VLM solver developed by Teixeira and Cesnik [22] based on Ref. [23] and is coupled to UM/NAST through an aerodynamic interface. The model consists of 36 panels in the spanwise direction and 18 panels in the chordwise direction. This discretization is based on a previously developed VLM model of the Technion Pazy wing [9, 10]. Dynamic aeroelastic solutions consider a prescribed wake model with a cut-off distance for discarding wake panels downstream of the wing equal to 2 m (20 chord lengths). The (U)VLM aerodynamic model adds 648 aerodynamic DOFs in static aeroelastic calculations corresponding to the circulations on the wing panels. Dynamic aeroelastic calculations add additional 7164 DOFs corresponding to circulations along the wake. The beam structural model and (U)VLM model interface through a loosely coupled scheme that exchanges information at every numerical iteration or time step. Displacement interpolation and load transfer between the dissimilar structural and aerodynamic discretization uses linear interpolation.

[1] https://github.com/UM-A2SRL/AePW3-LDWG.git

Table 2: Natural frequency verification and validation.

	GVT [13]	SOL 103		UM/NAST	
Mode type	Freq. (Hz)	Freq. (Hz)	Δ_{Test}	Freq. (Hz)	Δ_{FEM}
Out-of-plane bending (OOP1)	3.20	3.43	7.16	3.43	−0.02
Out-of-plane bending (OOP2)	22.50	22.81	1.37	22.87	0.27
Torsion (T1)	29.50	31.29	6.06	31.09	−0.63
Out-of-plane bending (OOP3)	65.00	65.85	1.30	66.29	0.68
In-plane bending (IP1)	n.a.	106.29	n.a.	107.23	0.88
Torsion (T2)	119.70	118.29	−1.18	123.34	4.28

4 RESULTS

This section first establishes the UM/NAST models of the TU Delft Pazy wing. Next, it compares wing gust responses to gust inputs simulated using the UM/NAST models.

4.1 Structural Model Verification and Validation

The beam model of the TU Delft Pazy wing in UM/NAST is assessed by comparing its natural frequencies in undeformed shape with those of the parent built-up FEM (with rigid rod) obtained using SOL 103 [17] and with GVT data [13].

Table 2 shows the comparison. The quantity Δ_{Test} denotes the relative error between corresponding built-up FEM and GVT frequencies; the quantity Δ_{FEM} denotes the relative error between corresponding UM/NAST and built-up FEM frequencies. The discussion starts by the error of the built-up FEM frequencies relative to the GVT frequencies. The first built-up FEM of the TU Delft Pazy wing, reported in Ref. [13], presented a higher OOP1 frequency (+3%), lower OOP2 and OOP3 frequencies (−3%), and lower T1 and T2 frequencies (−5% and −12%). The errors for the IP frequency are unknown. The second built-up FEM presents a 7% higher OOP1 frequency, 1% higher OOP2 and OOP3 frequencies, 4% higher T1 frequency, and 8% lower T2 frequency. The version used in this work considered in Table 2 has similar OOP frequency errors because, as mentioned earlier, tip rod flexibility impacts bending frequencies slightly. However, making the tip rod rigid increases the T1 frequency error to about 6% and reduces the T2 frequency error to 1%. Overall, this built-up FEM has relatively high OOP1 and T1 errors compared with the GVT, of approximately 6%−7%, and low errors of about 1% for the other frequencies. The bending frequency errors mainly originate from the model updating conducted at TU Delft, while the torsion frequency errors partly originate from the rigid tip rod considered in this work. These two errors compensate for the T2 frequency, explaining the more accurate result compared with other frequencies.

Next, the discussion shifts to the comparison between the built-up FEM natural frequencies and the corresponding frequencies of the UM/NAST beam model. The beam model captures the first five natural frequencies of the built-up FEM with errors below 1%. This level of accuracy is consistent with the findings in Ref. [9] for the Technion Pazy wing. The higher error of approximately 4% for the T2 frequency is attributed to the relatively coarse spatial discretization of the beam reference axis. While this error could be improved by increasing the number of beam finite elements for the same equivalent stiffness properties, it is considered to be acceptable for the scope of this work. The frequency errors of the beam model compared with the GVT are constrained by the errors associated with the built-up FEM.

The modal assurance criterion (MAC) is also computed to ensure that the beam model accurately captures the built-FEM mode shapes. The MAC between corresponding mode shapes achieves values between 0.99 and 1. Overall, the UM/NAST beam structural model captures the modal scenario of the experimental model in its undeformed shape with the same accuracy as the parent built-up FEM while only requiring a small fraction of the DOFs.

The beam model is further verified by comparing its nonlinear static response with results for the built-up FEM analyzed using the Nastran nonlinear solver SOL 400 [19] and (for completeness) the linear solver SOL 101 [24]. The wing is loaded by its self-weight plus incremental masses up to 3 kg at the tip, which excite tip deflections up to 60% semispan. Following Refs. [6, 9], two cases are considered where the tip masses are at the tip half-chord point (pure bending) and 0.08 m behind the tip trailing edge (bending-torsion).

Figure 1 compares the static responses for the various models and solvers. Tip vertical displacements are compared at the half-chord point; the tip twist angles are recovered from the differential positions of the tip leading and trailing edges. The comparisons do not include the initial displacement or twist angle offset due to the self-weight with no tip mass. As previously mentioned, while the built-up FEM is dynamically representative of the TU Delft Pazy wing with skin, it has no skin shell elements and can be used in SOL 400. The tip vertical displacements from SOL 400 and UM/NAST overlap, whereas the linear SOL 101 results overshoot the static response beyond 10% semispan (as expected). The SOL 400 and UM/NAST twist angles show a maximum difference of about 7% for tip masses up to 1 kg (tip vertical displacements of 35% semispan).

Overall, the structural verification and validation results show that the beam structural model of the TU Delft Pazy wing in UM/NAST accurately captures the modal scenario and static response of the parent built-up FEM in a wide deflection range while requiring much fewer DOFs. These conclusions align with the findings for the Technion Pazy wing [9].

4.2 Aeroelastic Model Verification and Validation

The aeroelastic model of the TU Delft Pazy wing is assessed by comparing its sea-level static aeroelastic response with higher-order numerical solutions and with wind tunnel test results reported in Ref. [13].

The verification considers the static aeroelastic response for varying flow speed in the range $U = 0 \rightarrow 40$ m/s at the root angles of attack α_r = 5 deg, 10 deg. The higher-order linear solution used for verification in the small-deflection range involves the built-up FEM (with rigid rod) coupled with the linear VLM in the Nastran linear static aeroelastic solver SOL 144 [18]. The higher-order nonlinear solution is based on the built-up FEM analyzed in SOL 400 by applying converged aerodynamic loads from UM/NAST. Again, the built-up FEM represents the TU Delft Pazy wing with skin but does not have skin elements, allowing its use in SOL 400. The UM/NAST results based on corrected strip theory are also compared with the results for the UM/NAST-VLM model to assess the impact of approximating wingtip effects with variable aerodynamic properties. The analyses are conducted without considering gravity and include a 0.01-kg mass on the rod, 0.01 m behind the trailing edge. The numerical results are compared in terms of tip vertical displacements and deformed shapes recovered at the half-chord spanwise points. The deformed shapes are compared at three flow speeds selected to yield small deflections ($U = 20$ m/s), large deflections ($U = 30$ m/s), and very large deflection case ($U = 40$ m/s).

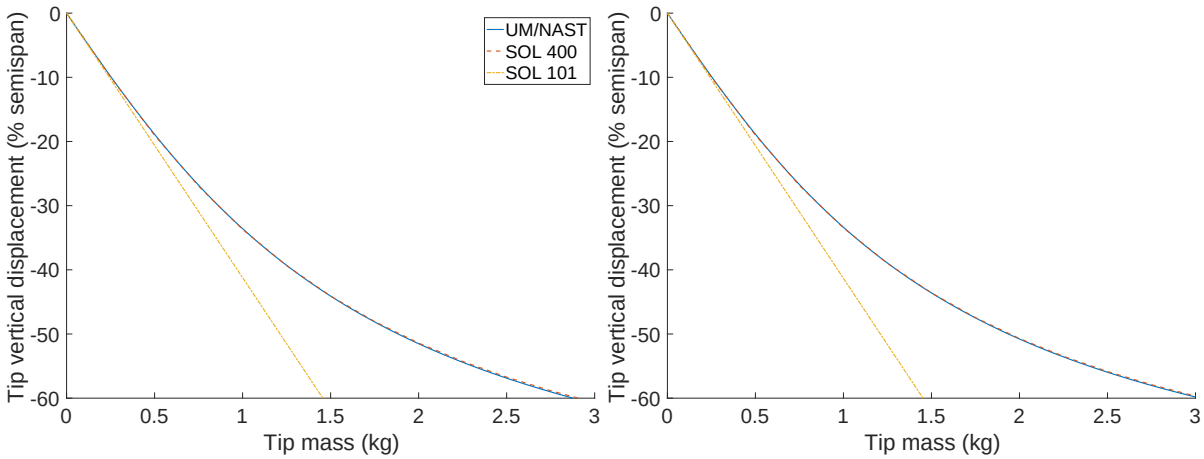

(a) Tip vertical displacement, pure bending case

(b) Tip vertical displacement, bending-torsion case

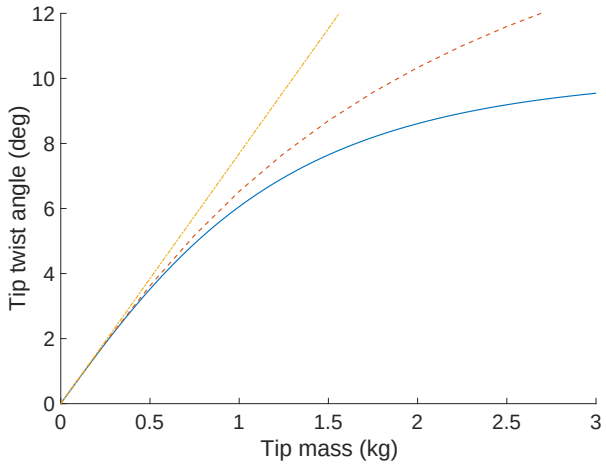

(c) Tip twist angle, bending-torsion case

Figure 1: Static structural response verification.

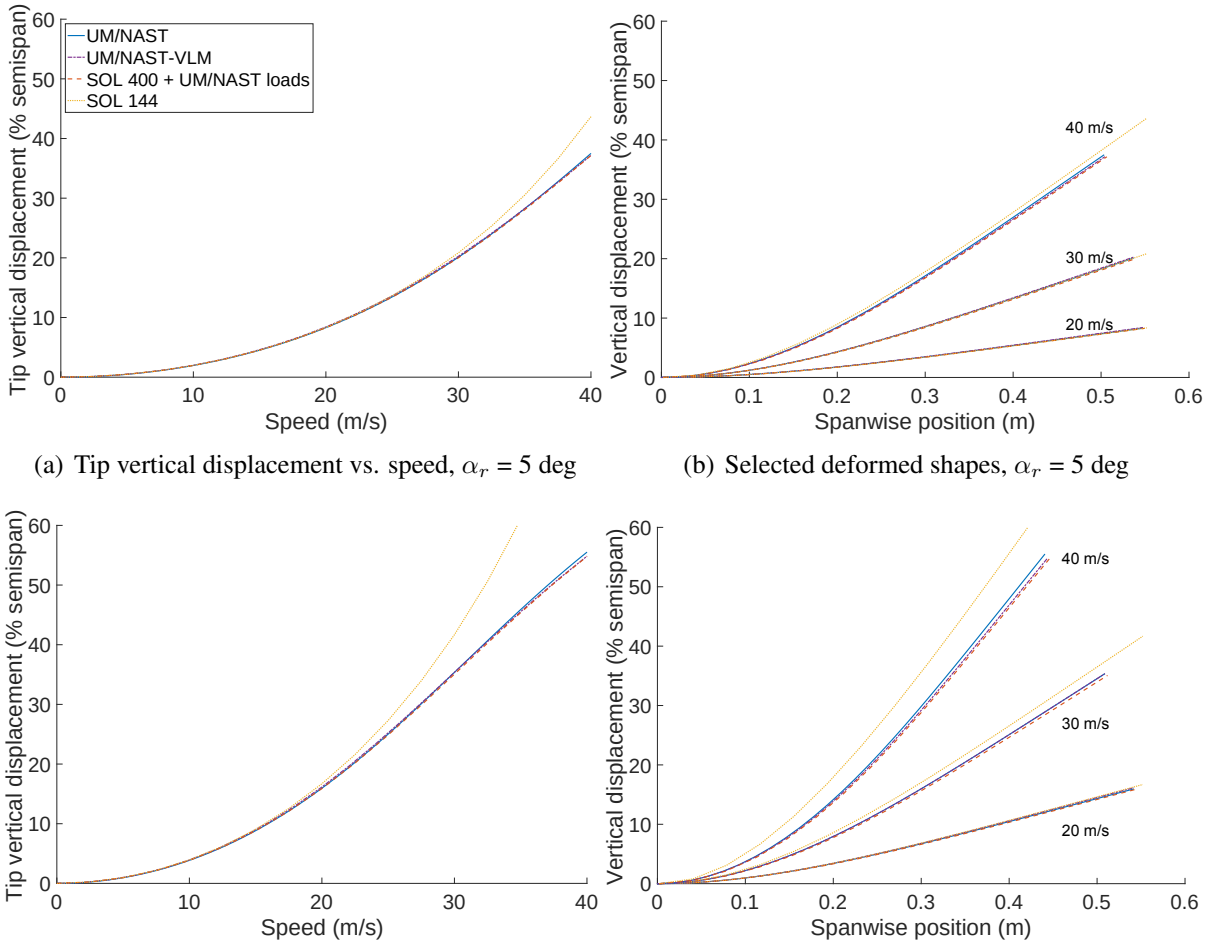

(a) Tip vertical displacement vs. speed, α_r = 5 deg

(b) Selected deformed shapes, α_r = 5 deg

(c) Tip vertical displacement vs. speed, α_r = 10 deg

(d) Selected deformed shapes, α_r = 10 deg

Figure 2: Static aeroelastic response verification.

Figure 2 compares the numerical results. The top line shows the static aeroelastic responses at the root angle of attack α_r = 5 deg. In the range of flow speeds considered, the nonlinear solutions yield maximum deflections of 35%−40% semispan. This deflection range is approximately double the one observed for the Technion Pazy wing [9] at the same operating conditions due to the higher flexibility of the TU Delft configuration. The results from all nonlinear models (UM/NAST, UM/NAST-VLM, and Nastran SOL 400) and the linear Nastran SOL 144 results overlap for deflections up to 15% semispan. The results from the nonlinear models remain in relatively close agreement [Fig. 2(a)] for higher tip deflections as well, with relative differences below 1.5% (see Table 3). However, the geometrically linear SOL 144 results neglect shortening effects at higher flow speeds and overshoot vertical displacements. The bottom line in Fig. 2 shows the static aeroelastic responses at the higher root angle of attack α_r = 10 deg. For this condition, the nonlinear and linear solutions yield maximum deflections of 55% and 85% semispan, respectively. The tip vertical displacements and deformed shapes from UM/NAST, UM/NAST-VLM, and SOL 400 remain in relatively close agreement even at extreme deflections [Fig. 2(c)], with relative differences below 2% (see Table 4). Overall, these results confirm the trends for the Technion Pazy wing [9, 10]. The low-order aeroelastic model based on the geometrically exact beam theory coupled with corrected strip theory accurately captures the static aeroelastic responses predicted by higher-order structural or aerodynamic formulations even at very large deflections, all while requiring a small fraction of the DOFs.

Table 3: Tip vertical displacements (% semispan) at α_r = 5 deg.

	SOL 400	UM/NAST-VLM		UM/NAST		
U (m/s)	Displ.	Displ.	Δ_{FEM} (%)	Displ.	Δ_{FEM}(%)	Δ_{VLM} (%)
20	8.27	8.41	1.74	8.30	0.32	−1.39
30	20.01	20.26	1.26	20.10	0.50	−0.75
40	37.16	37.17	0.03	37.50	0.90	0.87

Table 4: Tip vertical displacements (% semispan) at α_r = 10 deg.

	SOL 400	UM/NAST-VLM		UM/NAST		
U (m/s)	Displ.	Displ.	Δ_{FEM} (%)	Displ.	Δ_{FEM}(%)	Δ_{VLM} (%)
20	15.88	16.15	1.70	15.95	0.43	−1.25
30	35.06	35.87	0.88	35.37	0.86	−0.02
40	54.79	54.84	0.10	55.51	1.33	1.23

The validation with experimental results [13] focuses on the tip vertical displacement at the flow speed $U = 18.3$ m/s and root angles of attack α_r = 5 deg, 10 deg. At these operating conditions, the experimental tip vertical displacements remain below 15% semispan, a value for which results of different aeroelastic models closely agree. Therefore, the experimental results are only compared with the linear results from the built-up FEM model coupled with the VLM analyzed in SOL 144 and the nonlinear results from the low-order UM/NAST model with corrected strip theory aerodynamics. Table 5 shows the comparison. The high-order model analyzed in SOL 144 predicts lower tip vertical displacements compared with the experiments, with errors ranging from 19% at α_r = 5 deg to 13% at α_r = 10 deg. Because the tip deflections of the experimental model remain in a range where linear assumptions reasonably hold, these errors are attributed to the approximations associated with the built-up FEM updating. This explanation is based on Table 2, which shows that the built-up FEM has 6%−7% higher bending and torsional frequencies than the experimental model. At α_r = 5 deg, the results from SOL 144 and UM/NAST are within 0.4% of each other, confirming that the low-order model accurately captures the static aeroelastic response of the higher-order model while only requiring a small fraction of the DOFs. At α_r = 10 deg, the difference between SOL 144 and UM/NAST increases to approximately 3.5%. The UM/NAST model consistently predicts lower tip vertical displacements, which is attributed to the geometrically nonlinear formulation. However, the impact of geometrically nonlinear effects remains slight at the examined conditions. The accuracy of the low-order model in capturing the static aeroelastic response of the experimental model could be improved by further updating the parent built-up FEM used to derive the equivalent stiffness properties, which is the main error source. However, this is beyond the scope of this work.

Table 5: Tip vertical displacement (% semispan) at U = 18.3 m/s.

	Test [13]	SOL 144		UM/NAST		
α_r (deg)	Displ.	Displ.	Δ_{Test} (%)	Displ.	Δ_{Test}(%)	Δ_{FEM} (%)
5	8.50	6.90	−18.82	6.88	−19.12	−0.36
10	15.90	13.80	−13.21	13.31	−16.29	−3.55

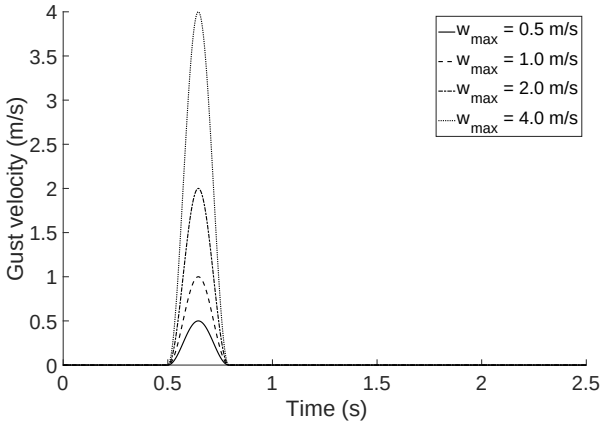

Figure 3: 1-cosine vertical gust velocity profiles.

4.3 Aeroelastic Gust Responses

This section compares gust responses predicted by UM/NAST and UM/NAST-UVLM. The analyses consider a discrete vertical gust input with no penetration and magnitude given by

$$w_{\text{gust}}(t) = \frac{w_{\max}}{2}\left[1 - \cos\left(\frac{2\pi t}{T}\right)\right] \tag{1}$$

The quantity $w_{\max}$ in Eq. (1) is the maximum gust velocity achieved at $t = T/2$, t is time, and T is the gust duration. The analyses consider a gust duration of $T = 0.29$ s that is selected based on the wing's OOP1 natural frequency of 3.43 Hz in the undeformed shape. Because the OOP1 frequency of the Pazy wing does not change significantly with the deformed shape [10], the chosen gust duration excites the lowest-frequency mode at all examined conditions. The gust input is incorporated into UM/NAST dynamic analyses by accounting for the instantaneous relative velocity contribution due to the gust when computing the local instantaneous effective angle of attack on each aerodynamic strip. For the UM/NAST-UVLM model, the gust input is incorporated by adding the contribution of the instantaneous gust velocity when applying the no-penetration boundary condition on different UVLM panels and when updating the wake convection with the contribution due to the gust perturbation.

The analyses consider two flow speeds U = 20 m/s, 30 m/s at root angles of attack α_r = 5 deg, 10 deg. These operating conditions are selected to be in the linearly stable regime of the TU Delft Pazy wing and to consider tip vertical deflections at equilibrium ranging from 8% to 35% semispan. The analyses focus on four gust inputs associated with maximum gust velocities $w_{\max}$ = 0.5 m/s, 1 m/s, 2 m/s, and 4 m/s (see Fig. 3). These gust velocities excite additional tip vertical deflections ranging from 3% to 30% semispan during the phase where the gust is active. Different combinations of maximum gust velocities, flow speeds, and root angles of attack allow the simulations to consider various levels of total aeroelastic deflections and different splits between the static and dynamic contributions. The gust responses from the UM/NAST and UM/NAST-UVLM models are compared in terms of the time histories of the tip vertical displacement at the half-chord point. Again, the analyses neglect gravity effects and include a 0.01-kg mass on the rod, 0.01 m behind the trailing edge. While experimental gust responses are available for the TU Delft model for a sinusoidal gust profile, the comparison here focuses on the results from the numerical models for a simpler gust input that is only active for a limited time duration. This gust input is selected to gain deeper insight into the impact of different aerodynamic models on the predicted aeroelastic dynamic responses when the gust is active and in the free decay to the original equilibrium state after the gust subsides.

Table 6: Maximum tip vertical displacements (% semispan) at U = 20 m/s and α_r = 5 deg.

	UM/NAST-UVLM Static displ. = 8.41	UM/NAST Static displ. = 8.30	
$w_{\max}$ (m/s)	Total displ.	Total displ.	Δ_{UVLM} (%)
0.5	11.74	11.57	−1.47
1.0	14.99	14.79	−1.33
2.0	21.19	21.04	−0.67
4.0	32.13	32.56	1.36

Table 7: Maximum tip vertical displacements (% semispan) at U = 20 m/s and α_r = 10 deg.

	UM/NAST-UVLM Static displ. = 16.15	UM/NAST Static displ. = 15.95	
$w_{\max}$ (m/s)	Total displ.	Total displ.	Δ_{UVLM} (%)
0.5	19.38	18.99	−2.03
1.0	22.38	21.94	−1.94
2.0	28.01	27.61	−1.41
4.0	37.73	37.81	0.25

Figures 4 to 7 compare the gust responses for different maximum gust velocities and operating conditions. In all cases, the gust starts at t = 0.5 s, and the shaded gray area shows the time interval during which it is active. Figure 4 compares the results at U = 20 m/s and α_r = 5 deg. The tip static vertical displacement at this operating condition is about 8% semispan, with additional maximum dynamic contributions ranging from 3% to 25% semispan. The total tip vertical displacement considering both the static and dynamic contributions lies in the range from a maximum of 35% to a minimum of −10% for the largest maximum gust velocity of 4 m/s. The UM/NAST-UVLM model yields a slightly larger static tip deflection (see Table 3) and the same holds for the incremental maximum deflection due to the gust, except for the case $w_{\max}$ = 4 m/s (see Table 6) where the UM/NAST-UVLM model predicts a slightly lower maximum deflection than UM/NAST. The relative differences between the maximum tip deflections predicted by the two models remain below 1.5% for all cases. Similar trends are observed at α_r = 10 deg in Fig. 5. The total tip vertical displacement considering both the static and dynamic contributions lies in the range from a maximum of 40% to a minimum of −0.5% for the largest maximum gust velocity of 4 m/s and the relative differences between the maximum tip deflections remain below 2%. While the two models are in close agreement during the phase where the gust is active, they show larger differences in the subsequent free decay for increasing maximum gust velocities. Specifically, the UM/NAST model predicts larger aerodynamic damping resulting in a faster recovery to the original equilibrium state compared with the UM/NAST-UVLM model, which yields a less damped response. This finding aligns with previous results for the Technion Pazy wing, for which strip theory corrected using the present approach overpredicted aerodynamic damping [10]. Figures 4 and 5 show no significant difference in the characteristic frequency associated with the free decay and no phase shift. This result can be explained considering that the aeroelastic frequencies of the wing are dictated by the deformed shape at equilibrium for each operating condition, which is similar between the UM/NAST and UM/NAST-UVLM models [10].

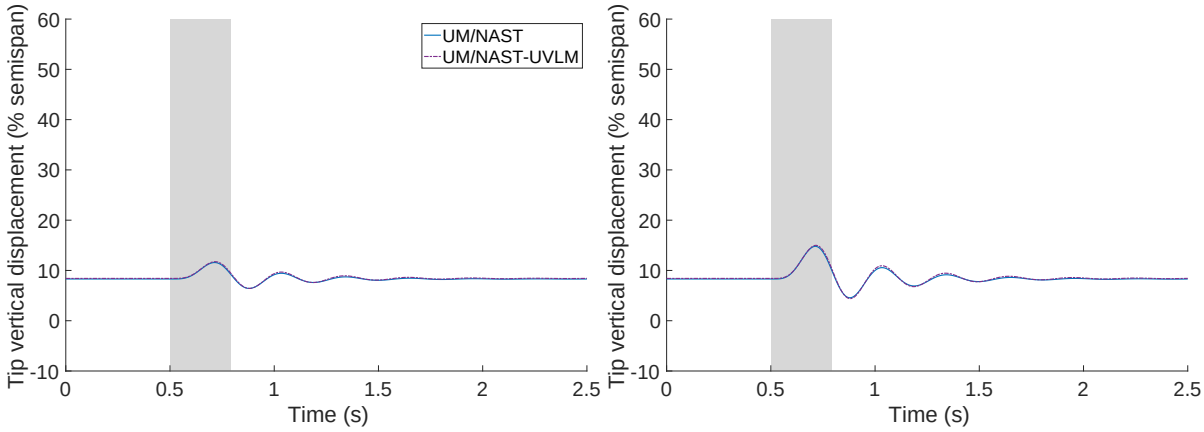

(a) $w_{\max}$ = 0.5 m/s

(b) $w_{\max}$ = 1 m/s

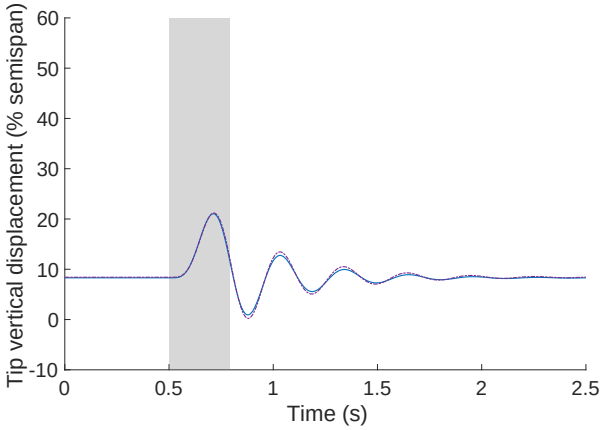

(c) $w_{\max}$ = 2 m/s

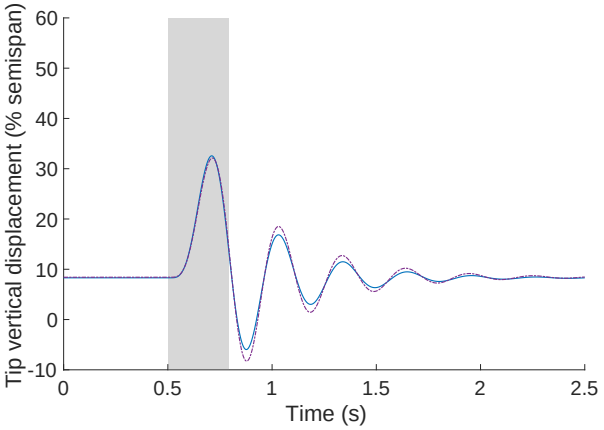

(d) $w_{\max}$ = 4 m/s

Figure 4: Gust responses at U = 20 m/s and α_r = 5 deg.

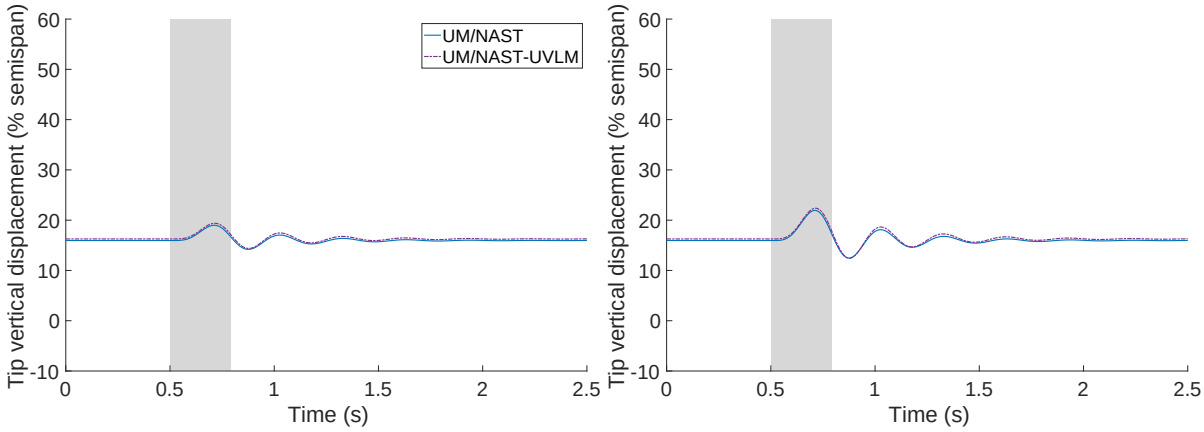

(a) $w_{\max}$ = 0.5 m/s

(b) $w_{\max}$ = 1 m/s

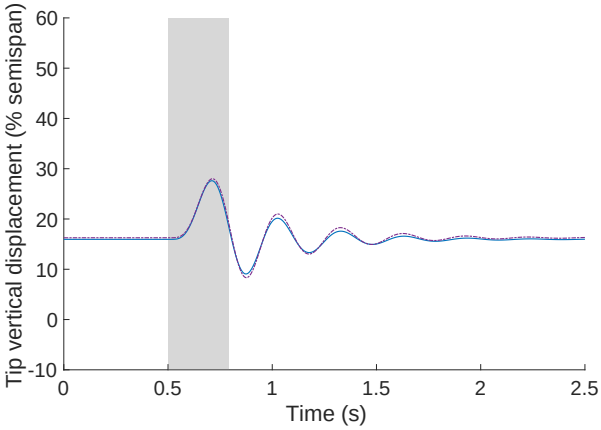

(c) $w_{\max}$ = 2 m/s

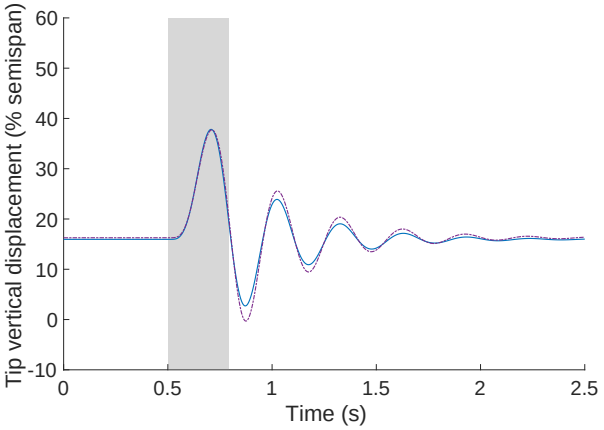

(d) $w_{\max}$ = 4 m/s

Figure 5: Gust responses at U = 20 m/s and α_r = 10 deg.

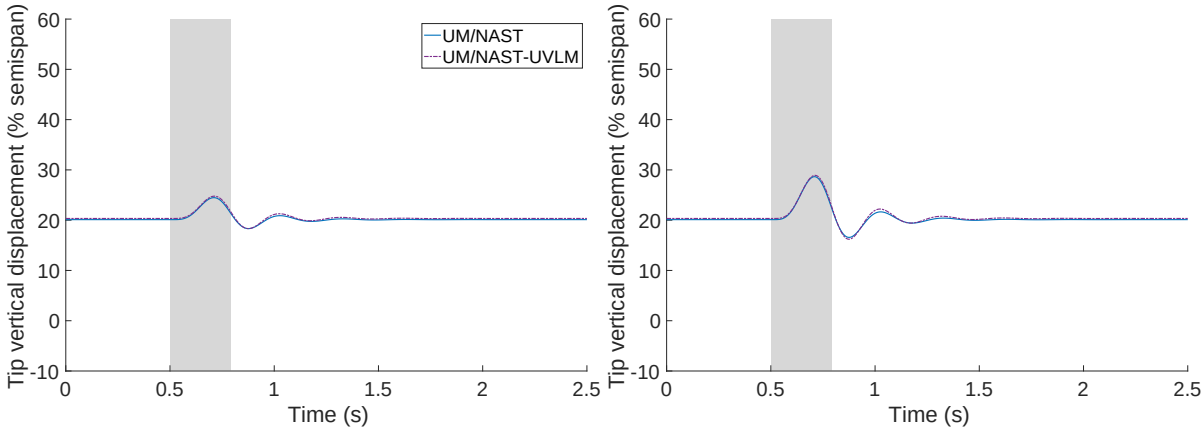

(a) $w_{\max}$ = 0.5 m/s

(b) $w_{\max}$ = 1 m/s

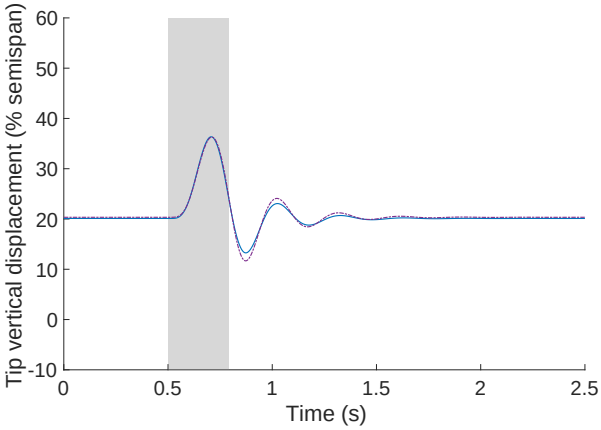

(c) $w_{\max}$ = 2 m/s

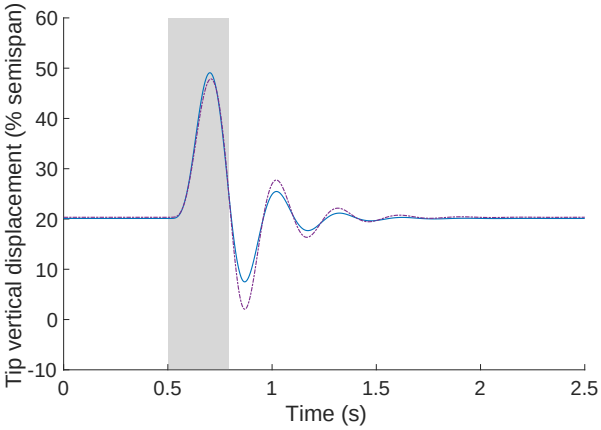

(d) $w_{\max}$ = 4 m/s

Figure 6: Gust responses at U = 30 m/s and α_r = 5 deg.

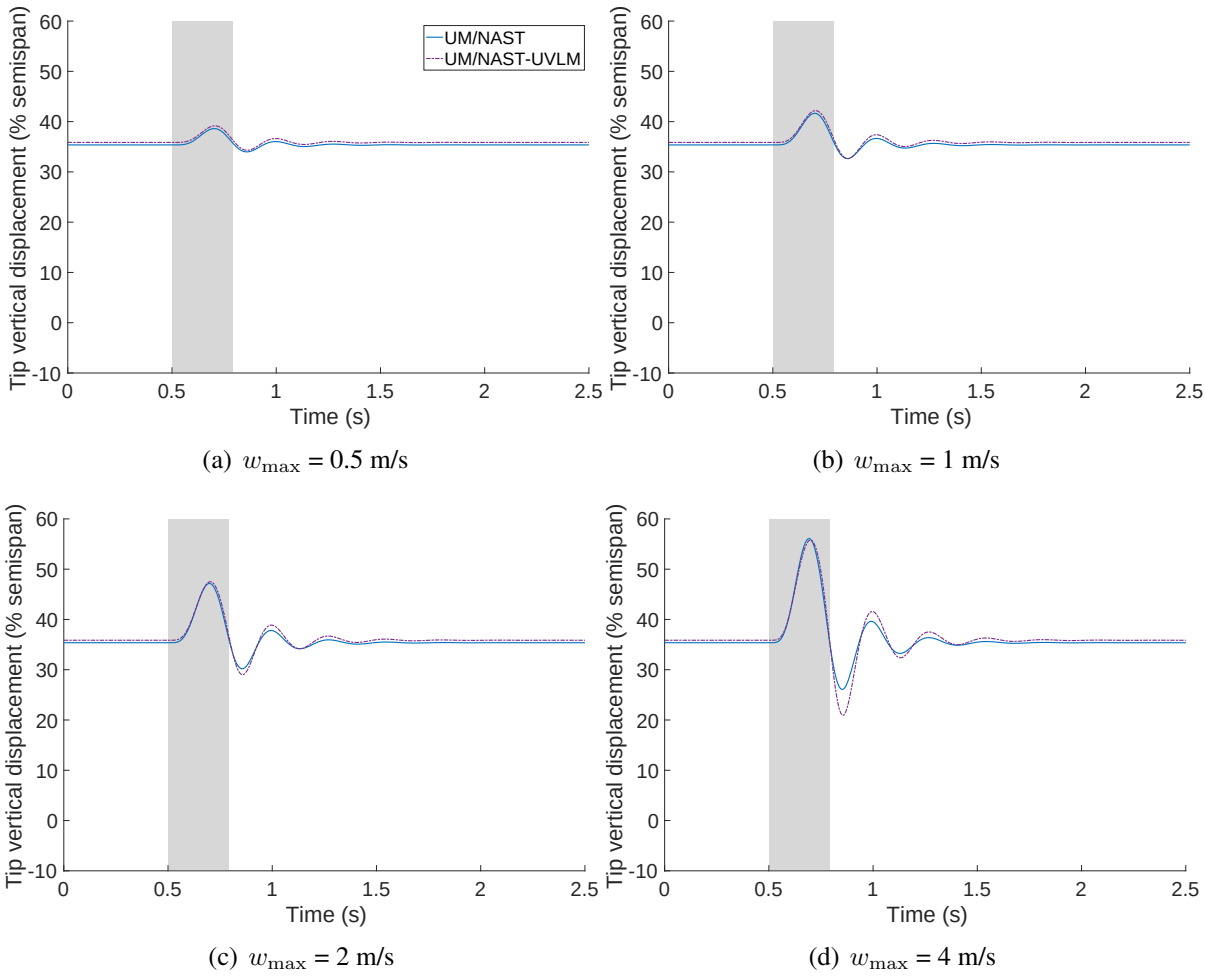

(a) $w_{\max}$ = 0.5 m/s

(b) $w_{\max}$ = 1 m/s

(c) $w_{\max}$ = 2 m/s

(d) $w_{\max}$ = 4 m/s

Figure 7: Gust responses at U = 30 m/s and α_r = 10 deg.

Table 8: Maximum tip vertical displacements (% semispan) at α_r = 5 deg and U = 30 m/s.

	UM/NAST-UVLM Static displ. = 20.26	UM/NAST Static displ. = 20.10	
$w_{\max}$ (m/s)	Total displ.	Total displ.	Δ_{UVLM} (%)
0.5	24.78	24.48	−1.20
1.0	28.91	28.65	−0.91
2.0	36.29	36.35	0.17
4.0	47.86	49.09	2.56

Table 9: Maximum tip vertical displacements (% semispan) at α_r = 10 deg and U = 30 m/s.

	UM/NAST-UVLM Static displ. = 35.87	UM/NAST Static displ. = 35.37	
$w_{\max}$ (m/s)	Total displ.	Total displ.	Δ_{UVLM} (%)
0.5	39.16	38.61	−1.41
1.0	42.18	41.65	−1.26
2.0	47.49	47.16	−0.71
4.0	55.80	56.09	0.53

Next, Figs. 6 and 7 compare the results at U = 30 m/s for α_r = 5 deg, 10 deg. At these operation conditions, the tip total vertical displacements reach 55% semispan (see Tables 8 and 9) with a dynamic contribution up to 30% semispan. Despite these larger static and dynamic deflections, the relative differences between the maximum tip vertical displacements predicted by the UM/NAST and UM/NAST-UVLM models remain below 3%. This slightly larger difference compared with the case U = 20 m/s partly stems from the tip vertical displacement at equilibrium, which is slightly larger for the UM/NAST-UVLM model (which becomes a UM/NAST-VLM model in static aeroelastic analyses).

Similar to the results at the lower flow speed in Figs. 4 and 5, the UM/NAST model predicts a higher aerodynamic damping in the free response after the gust subsides, with more pronounced differences compared with UM/NAST-UVLM for increasing maximum gust velocities. Larger maximum gust velocities excite larger dynamic deflections for the same static deflection, accentuating aerodynamic damping differences in the two models. Based on the remarks from previous flutter analyses for the Technion Pazy wing [10], this behavior can be explained by considering that the correction for wingtip effects in the UM/NAST strip theory formulation is based on spanwise varying aerodynamic coefficient derivatives. These aerodynamic coefficient derivatives are obtained from a rigid panel method steady aerodynamic analysis of the undeformed wing at a 1-deg root angle of attack and are therefore not necessarily representative of three-dimensional aerodynamic effects during dynamic responses at highly deflected conditions. As a result, accounting for wingtip effects by using spanwise varying aerodynamic properties in the strip theory model is suitable to capture the impact of these effects on the static aeroelastic deflection at equilibrium while avoiding a fully three-dimensional aerodynamic analysis based on a more sophisticated aerodynamic formulation such as the UVLM. However, it introduces approximations in dynamic analyses such as those associated with gust responses compared with the use of a true three-dimensional unsteady aerodynamic model.

Overall, the UM/NAST model based on corrected strip theory captures the overall behavior of the wing during the gust response even at extreme levels of aeroelastic deflection. As mentioned earlier, the model accurately predicts the peak tip vertical displacement during the gust as well as the frequency and phase of the subsequent free response. The model yields significantly faster gust response simulations compared with the use of UVLM, which adds a significantly larger number of aerodynamic DOFs to the problem compared with the 90 DOFs associated with the strip theory model used in this work.

5 CONCLUDING REMARKS

This paper compared the gust responses of a very flexible wing predicted using geometrically nonlinear aeroelastic models of different levels of complexity. The paper built and expanded on previous studies under the AePW3 LDWG focused on understanding the ability of different aeroelastic models to predict modal, static, and flutter characteristics of very flexible wings. This study focused on the Pazy wing developed at TU Delft for gust response experiments in low-speed flow. Gust response simulations were conducted in the UM/NAST framework using two aeroelastic models. These models consisted of a common geometrically exact strain-based beam representation of the parent built-up FEM coupled with unsteady potential flow aerodynamic models based on either corrected strip theory (low-order UM/NAST model) or the UVLM (medium-order UM/NAST-UVLM model). After verifying and validating the models, the study examined wing responses to a 1-cosine vertical gust profile for various maximum gust velocity magnitudes and operating conditions exciting a wide range of static, dynamic, and total deflections.

The UM/NAST and UM/NAST-UVLM models were found to predict similar maximum tip vertical displacements during the gust encounter, with small differences up to 3% even at extreme deflections up to 55% semispan. Part of these differences originated from the different static aeroelastic deflections, which were slightly larger for the second model. Additionally, the two models predicted similar characteristic frequencies and phases in the free decay after the gust subsided. However, the UM/NAST model based on corrected strip theory overpredicted aerodynamic damping in the free decay, consistent with previous flutter predictions for the Technion Pazy wing. The overestimated damping resulted from the use of spanwise varying aerodynamic coefficient derivatives from steady rigid calculations to account for wingtip effects in gust response simulations, and was exacerbated in the presence of increasing dynamic deflections. Regardless, the UM/NAST model was found to capture the overall wing gust response behavior while requiring a relatively low number of DOFs.

Future work will further investigate the ability of different aeroelastic models to predict the gust response of very flexible wings for 1-cosine gust profiles exciting other frequencies than the one considered here, whose duration was tuned on the frequency of the first bending mode. Additional comparisons with the Nastran gust response solver SOL 146 will be conducted to further assess the present aeroelastic models for small deflections. Finally, comparisons with the TU Delft experimental data for sinusoidal gust encounters will be conducted to validate the model for the dynamic response cases and investigate their ability to predict the responses of the experimental wing.

ACKNOWLEDGMENTS

The authors thank Dr. Christoph Mertens (NLR) for sharing the TU Delft Pazy built-up FEM used at the starting point for creating the UM/NAST model used in this study.

6 REFERENCES

[1] Afonso, F., Vale, J., Oliveira, É., et al. (2017). A review on non-linear aeroelasticity of high aspect-ratio wings. *Progress in Aerospace Sciences*, 89, 40–57. doi:10.1016/j.paerosci.2016.12.004.

[2] Ma, Y. and Elham, A. (2024). Designing high aspect ratio wings: A review of concepts and approaches. *Progress in Aerospace Sciences*, 145, 100983. doi:https://doi.org/10.1016/j.paerosci.2024.100983.

[3] Afonso, F., Sohst, M., Diogo, C. M., et al. (2023). Strategies towards a more sustainable aviation: A systematic review. *Progress in Aerospace Sciences*, 137, 100878. doi:https://doi.org/10.1016/j.paerosci.2022.100878.

[4] Cesnik, C. E. S., Palacios, R., and Reichenbach, E. Y. (2014). Reexamined structural design procedures for very flexible aircraft. *Journal of Aircraft*, 51(5), 1580–1591. doi:10.2514/1.C032464.

[5] Ritter, M., Hilger, J., Ribeiro, A. F. P., et al. (2024). Collaborative pazy wing analyses for the third aeroelastic prediction workshop. In *AIAA SciTech Forum*. Orlando, FL, pp. 1–24. doi:10.2514/6.2024-0419. AIAA-2024-0419.

[6] Avin, O., Raveh, D. E., Drachinsky, A., et al. (2022). Experimental aeroelastic benchmark of a very flexible wing. *AIAA Journal*, 1–24. doi:10.2514/1.J060621. Article in advance.

[7] Tang, D. and Dowell, E. H. (2001). Experimental and theoretical study on aeroelastic response of high-aspect-ratio wings. *AIAA Journal*, 39, 1430–1441. doi:10.2514/2.1484.

[8] Drachinsky, A., Avin, O., Raveh, D. E., et al. (2022). Flutter tests of the pazy wing. *AIAA Journal*, 1–8. doi:10.2514/1.J061717. Article in advance.

[9] Riso, C. and Cesnik, C. E. S. (2023). Impact of low-order modeling on aeroelastic predictions for very flexible wings. *Journal of Aircraft*, 60(3), 662–687. doi:10.2514/1.C036869.

[10] Riso, C. and Cesnik, C. E. S. (2023). Geometrically nonlinear effects in wing aeroelastic dynamics at large deflections. *Journal of Fluids and Structures*, 120(July), 1–27. doi:10.1016/j.jfluidstructs.2023.103897.

[11] del Carre, A., noz Simón, A. M., Goizueta, N., et al. (2019). SHARPy: A dynamic aeroelastic simulation toolbox for very flexible aircraft and wind turbines. *Journal of Open Source Software*, 4(44), 1885. doi:10.21105/joss.01885.

[12] Ribeiro, A. F., Casalino, D., and Ferreira, C. (2023). Free wake panel method simulations of a highly flexible wing in flutter and gusts. *Journal of Fluids and Structures*, 121, 103955. doi:https://doi.org/10.1016/j.jfluidstructs.2023.103955.

[13] Mertens, C., Costa Fernández, J. L., Sodja, J., et al. (2023). Nonintrusive experimental aeroelastic analysis of a highly flexible wing. *AIAA Journal*, 61(7), 3062–3077. doi:10.2514/1.J062476.

[14] Su, W. and Cesnik, C. E. S. (2010). Nonlinear aeroelasticity of a very flexible blended-wing-body aircraft. *Journal of Aircraft*, 47(5), 1539–1553. doi:10.2514/1.47317.

[15] Su, W. and Cesnik, C. E. S. (2011). Strain-based geometrically nonlinear beam formulation for modeling very flexible aircraft. *International Journal of Solids and Structures*, 48(16–17), 2349–2360. doi:10.1016/j.ijsolstr.2011.04.012.

[16] Cesnik, C. E. S. and Hodges, D. H. (1997). VABS: A new concept for composite rotor blade cross-sectional modeling. *Journal of the American Helicopter Society*, 42(1), 27–38. doi:10.4050/jahs.42.27.

[17] Anon. (2017). *MSC Nastran Dynamic Analysis User's Guide*. MSC Software Corporation.

[18] Anon. (2017). *MSC Nastran Aeroelastic Analysis User's Guide*. MSC Software Corporation.

[19] Anon. (2016). *MSC Nastran Non Linear User's Guide SOL400*. MSC Software Corporation.

[20] Riso, C., Sanghi, D., Cesnik, C. E. S., et al. (2020). Parametric roll maneuverability analysis of a high-aspect-ratio-wing civil transport aircraft. In *AIAA SciTech Forum*. Orlando, FL, pp. 1–23. doi:10.2514/6.2020-1191. AIAA-2020-1191.

[21] Peters, D. A., Hsieh, M. C. A., and Torrero, A. (2007). A state-space airloads theory for flexible airfoils. *Journal of the American Helicopter Society*, 52(4), 329–342. doi:10.4050/JAHS.52.329.

[22] Teixeira, P. C. and Cesnik, C. E. S. (2019). Propeller effects on the response of high-altitude long-endurance aircraft. *AIAA Journal*, 57(10), 4328–4342. ISSN 00011452. doi:10.2514/1.J057575.

[23] Ritter, M., Cesnik, C. E. S., and Krüger, W. R. (2015). An enhanced modal approach for large deformation modeling of wing-like structures. In *AIAA SciTech Forum*. Kissimmee, FL, pp. 1–16. doi:10.2514/6.2015-0176. AIAA 2015-0176.

[24] Anon. (2017). *MSC Nastran Linear Static Analysis User's Guide*. MSC Software Corporation.

COPYRIGHT STATEMENT